Materials Advances

ROYAL SOCIETY OF CHEMISTRY

COMMUNICATION

View Article Online
View Journal | View Issue

Cite this: *Mater. Adv.*, 2024, 5, 1868

Received 16th September 2023,
Accepted 7th February 2024

DOI: 10.1039/d3ma00716b

rsc.li/materials-advances

The Gore-Tex® effect in externally hydrophobic Metal–Organic Frameworks†

Kaleb L. Miller, [b] Rijia Lin, [c] Jingwei Hou, [c] Cameron J. Kepert, *[b] Deanna M. D'Alessandro *[ab] and Marcello B. Solomon *[ab]

UiO-66-NH_2 ($[Zr_6O_4(OH)_4(NH_2\text{-bdc})]$, NH_2-bdc = 2-aminoterephthalic acid) was post-synthetically modified using four strategies to improve its external hydrophobicity. The modified MOFs exhibited increased hydrophobicity to water droplets, but their internal hydrophobicity remained unchanged. This highlights a disconnect between hydrophobicity towards vapour and liquid water, referred to as the Gore-Tex® effect.

Introduction

Since their discovery over 30 years ago, Metal–Organic Frameworks (MOFs) have been earmarked as a class of materials capable of revolutionising the CO_2 capture, storage and removal industries.[1–3] Their potential applications continue to grow as new architectures are discovered. Sustained efforts in MOF syntheses have enabled experimental internal surface areas of up to 6550 m^2g^{-1} to be reached.[1,4] Theoretically, the surface areas of MOF materials can reach beyond 14 000 m^2g^{-1}.[5] High surface areas and accessible pore spaces have enabled the pores of MOFs to play host to a variety of functional chemistries, including fine chemical production,[6] sensing[7] and gas separations.[8] MOFs are well studied on the laboratory bench; however, translating their technology to the industrial scale requires further scrutiny. Of the 90 000+ architectures reported to date,[9] only a few MOFs have been documented for their commercial use.[10,11]

When MOFs are evaluated for their suitability to capture CO_2 under laboratory conditions, many industrially relevant conditions are irreplicable or may be overlooked. An important factor in the laboratory is the overall CO_2 capacity that a material may possess; however, this is normally determined through thermodynamic measurements under equilibrium conditions by slowly dosing in CO_2 to an evacuated sample of material.[12] Selectivity – the extent in which a material can favour particular analytes in mixtures without interference from other components[13] – is usually determined in the laboratory from a two-component gas mixture under dry conditions,[14] or from competitive breakthrough experiments.[15,16] In real world conditions, high selectivity for CO_2 over multiple gases (N_2, O_2, H_2O, SO_x, NO_x among others) is often crucial for the performance of a CO_2 capture material. The MOF material may also need to operate under non-ideal conditions, such as at elevated temperatures, increased pressures and humid gas streams. A particular industrial challenge is the competitive binding between CO_2 and H_2O for a solid-state adsorbent. H_2O often adsorbs preferentially to CO_2 due to its ability to form extensive hydrogen bonding with the MOF, or with itself within the MOF pores, thus reducing the capacity for CO_2.[17] Furthermore, many MOFs suffer from their sensitivity to moisture and may degrade upon exposure to atmospheric H_2O. The archetypal framework MOF-5 ($[ZnO_4(bdc)_3]$ bdc = 1,4-benzenedicarboxylate) has reported surface areas of 3800 m^2g^{-1} and pore volumes of 1.55 $cm^3\ g^{-1}$; however, its hydrolytic instability makes it unsuitable in applications involving humid air as the H_2O breaks down the framework.[18,19] Improving the hydrophobicity of a MOF is hypothesised to surmount some of these fundamental challenges.

Endowing a MOF with innate hydrophobicity, or introducing a hydrophobic composite material into a MOF may help diminish the detrimental impact of H_2O on a pristine framework.[20,21] Hydrophobic porous materials are gaining interest for reducing the competition between CO_2 and H_2O for their deployment into the gas capture and storage field under humid conditions.[8,22–25] Hydrophobicity can be achieved *via* one of three pathways: (1) deliberate pre-synthetic design using ligands with hydrophobic properties, although predesigned hydrophobicity may not guarantee that the resultant framework will be hydrophobic, since the metal secondary

[a] *School of Chemical and Biomolecular Engineering, The University of Sydney, New South Wales 2006, Australia*
[b] *School of Chemistry, The University of Sydney, New South Wales 2006, Australia. E-mail: cameron.kepert@sydney.edu.au, deanna.dalessandro@sydney.edu.au, marcello.solomon@sydney.edu.au*
[c] *School of Chemical Engineering, The University of Queensland, Queensland 4072, Australia*

† Electronic supplementary information (ESI) available. See DOI: https://doi.org/10.1039/d3ma00716b

building unit (SBU) of the framework may bind H_2O;[26] (2) *in situ* functionalisation of the ligand or SBU to generate an intrinsically hydrophobic MOF;[27] or (3) bestowing hydrophobicity through post-synthetic modification (PSM)[28] *via* ligand or metal-ion exchange, ligand functionalisation, or guest introduction.[29] The benefit of PSM is the ability to produce functional MOFs in a simple, inexpensive and scalable way, which is an enticing pathway towards their industrial deployment.

Porous materials possess two types of hydrophobicity: internal and external hydrophobicity.[30,31] Internal hydrophobicity is defined by the adsorption of water vapour to the internal pore surface of a porous material (as influenced by the competition between weak favourable enthalpic water–surface interactions and unfavourable adsorption entropies), while external hydrophobicity concerns the interaction of liquid H_2O at the surface of the material (relating principally to the dominance of water–water over water–surface interaction enthalpies). External hydrophobicity acts on a macroscopic scale compared to internal hydrophobicity and is generally characterised by a water contact angle measurement. Their distinction is essential given that hydrophobic porous materials are used for applications concerning both liquid and gaseous H_2O. A challenge arises when measurements for external hydrophobicity are extrapolated to make assumptions about the internal hydrophobicity of a material.[30,32] Computational studies performed by Snurr *et al.* suggest that hydrophobicity indicated by the external water contact angle does not correlate with the hydrophobicity of the internal pore environments, indicated by vapour sorption.[30] Porous materials may exhibit external hydrophobicity without exhibiting internal hydrophobicity, similar to Gore-Tex®[33] – the material used in hydrophobic clothing.[30]

External hydrophobicity, as measured by the water contact angle, is frequently assumed to be a reliable metric for characterising the performance of MOFs under humid conditions;[23,34–37] however, this is not the case. To the best of our knowledge, we present here the first study which practically demonstrates the differences between internal and external hydrophobicity in MOFs. We explore and apply four hydrophobic PSMs to UiO-66-NH_2 – a readily scalable MOF that can be synthesised *via* green pathways.[38] These hydrophobic PSMs include: (1) Enteric coatings – a widespread, cheap class of polymers used in the pharmaceutical industry to protect medications as they pass through the human digestive system,[39–41] and have recently found effectiveness in imparting hydrophobicity to MOFs;[42] (2) Long-chained alkanes with a terminal group enabling post-synthetic modification to the SBU of a MOF or reaction with a ligand – these have been well studied in their improvement in the stability of MOFs to water;[43,44] (3) Organosilicon infiltration – where cheap, commercially available organosilicone-based materials[8,24] can create a hydrophobic layer on the exterior surface of the MOF to improve its stability to water; and (4) SBU modification, which may proceed by dative coordination of molecules to unsaturated SBUs.[29,45]

Results and discussion

Development of PSM strategies and synthesis of UiO-66-NH_2

UiO-66-NH_2 was successfully synthesised according to the literature methodology, with PXRD and Le Bail data matching that previously reported (Fig. S1 and Table S1, ESI†). SEM images are also consistent with previously reported micrograms (Fig. S2, ESI†).[46] Each of the four strategies (Fig. 1) were tested on the same batch of UiO-66-NH_2, allowing for their direct comparison.

Strategy one: external hydrophobicity using enteric coatings. Four enteric polymers were evaluated for improving the hydrophobicity of MOFs: hydroxypropyl methylcellulose phthalate (HPMCP), Acryl-Eze®, Sureteric® and Eudragit RL®. The best

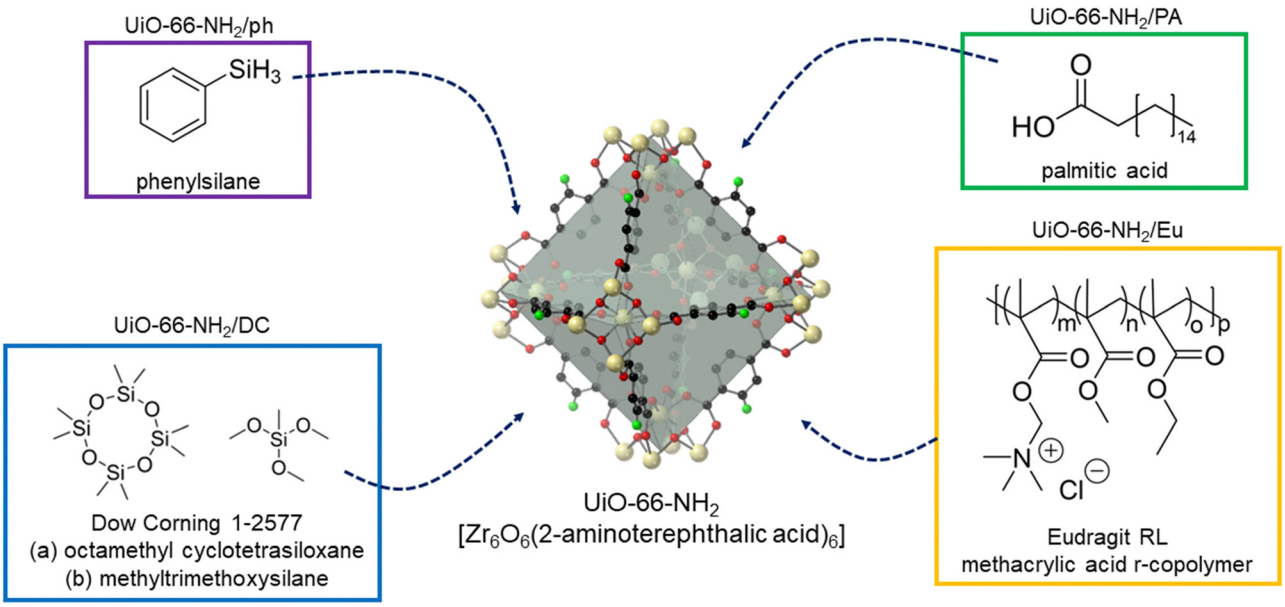

Fig. 1 The four post-synthetic modification strategies used to endow UiO-66-NH_2 with hydrophobicity.

performing enteric polymer coating was Eudragit RL® (Fig. S3, ESI†), which exhibited a hydrophobic contact angle of ~134°. Solutions of Eudragit RL® (0.5, 1, 2, 5 and 8 wt%) were prepared to determine the optimal coating of Eudragit RL®, which coated the UiO-66-NH_2 over three hours. The concentration of Eudragit RL® did not affect the contact angle but increased the time the droplet remained intact on the surface (Fig. S4, ESI†). The 5 wt% sample was the lowest concentration of enteric coating that enabled the water droplet to remain intact for the longest period, which is attributed to a more uniform hydrophobic coating. Minimising the enteric coating thickness while maintaining hydrophobicity allowed for preservation of gas adsorption properties. Spectroscopic characterisation confirmed the presence of Eudragit RL® on the framework surface (Table S2 and Fig. S5–S8, ESI†). This material will be referred to herein as UiO-66-NH_2/Eu.

Strategy two: external hydrophobicity using long-chained alkane PSM. The long-chained alkanes octadecyl amine, magnesium stearate and palmitic acid (PA) (Fig. S9, ESI†) were chosen as candidates to improve the hydrophobicity of UiO-66-NH_2.[43,44] PA was the only candidate which yielded a hydrophobic contact angle (129°). The duration of coating was varied between 30 minutes and 16 hours; however, no time dependence of coating duration on the contact angle was observed. A coating time of three hours was chosen to ensure a sufficiently uniform composite layer coating of 2%. The inclusion of PA was confirmed through the structural characterisation of the material (Table S3 and Fig. S10–S13, ESI†). This material will be referred to herein as UiO-66-NH_2/PA.

Strategy three: external hydrophobicity using commercially available silane-based hydrophobic agents. Hydrophobic silane coating materials are ubiquitous in the literature, with many commercial waterproofing sealants on the market.[20,23,47] Due to its ready commercial availability, DOWSIL™ 1-2577 Conformal (DC) coating was chosen as a candidate silane to coat UiO-66-NH_2. The active hydrophobic agents in DC (Fig. S14, ESI†) are large and unlikely to infiltrate the pores of UiO-66-NH_2; therefore, the coating is only expected to interact with the external MOF surface *via* van der Waals forces.[48,49] The 8 wt% loading of DC was chosen to minimise layer thickness and maximise external hydrophobicity without impacting on accessible surface area. Structural characterisation of the composite material indicated that DC could coat the MOF without impacting its structural features (Fig. S15–S18, ESI†). This material will be referred to herein as UiO-66-NH_2/DC.

Strategy four: internal hydrophobicity using phenylsilane grafting. Phenylsilane (Fig. S19, ESI†) has previously been grafted onto the SBU of UiO-66-NH_2, which occurred *via* a silylation reaction performed in acetonitrile and Cs_2CO_3 under a CO_2 atmosphere.[29,50] The silylation reaction was confirmed by a colour change of the pristine UiO-66-NH_2 from pale yellow to a bright yellow upon grafting. Preservation of the structure of the grafted MOF following phenylsilane incorporation was confirmed (Fig. S20–S23, ESI†). This material will be referred to herein as UiO-66-NH_2/ph.

Gas sorption studies. The porosity of the optimised hydrophobic samples was evaluated through N_2 gas sorption measurements performed at 77 K (Fig. 2). Pristine UiO-66-NH_2 and all derivatives except UiO-66-NH_2/DC exhibited Type I(b) isotherms, which is typical for microporous materials.[51] UiO-66-NH_2/DC exhibited a Type IV(a) isotherm with hysteresis.[51] Hysteresis is typically associated with the filling of wide pores through a narrow surface opening – it may be that the DOWSIL™ coating blocks the entrance to the pores of the framework, hindering the adsorption and desorption of N_2.

Brunauer–Emmett–Teller (BET) surface areas were calculated for each sample.[52] Pristine UiO-66-NH_2 had a BET surface area of 1054 ± 19 m^2g^{-1}, which is consistent with literature reports (Table S4, ESI†).[53,54] Post-synthetic modifications of the framework caused the reduction in surface area to varying degrees. The most significant reduction in surface area was to UiO-66-NH_2/ph, where a BET surface area of 66 ± 1 m^2g^{-1} was determined. It is likely that the phenylsilane grafting onto the zirconium SBU caused blocking of the framework pore windows from the aromatic ring. This was supported by pore volume measurements, which indicate a reduction from 0.44 to 0.03 $cm^3\ g^{-1}$. The DOWSIL™ coating resulted in a surface area reduction to 465 ± 6 $m^2\ g^{-1}$, which is attributable to pore infiltration of the smaller active hydrophobic agents. The pore volume reduced from 0.44 to 0.19 $cm^3\ g^{-1}$, confirming a degree of pore blocking by the organosilicon. The polymeric derivatives, UiO-66-NH_2/Eu and UiO-66-NH_2/PA, yielded surface areas of 779 ± 9 $m^2\ g^{-1}$ and 759 ± 9 $m^2\ g^{-1}$, respectively, with respective pore volume reductions to 0.30 and 0.31 $cm^3\ g^{-1}$. This suggests that the long-chained nature of the coating agents still allows for adsorption to occur.

Pore size distribution data from gas sorption measurements demonstrate the impact of PSM on the parent UiO-66-NH_2 framework (Fig. S24, ESI†). The pristine UiO-66-NH_2 exhibits two different sized micropores (16 Å and 18.5 Å). UiO-66-NH_2/Eu and UiO-66-NH_2/DC both reveal a reduction in the larger

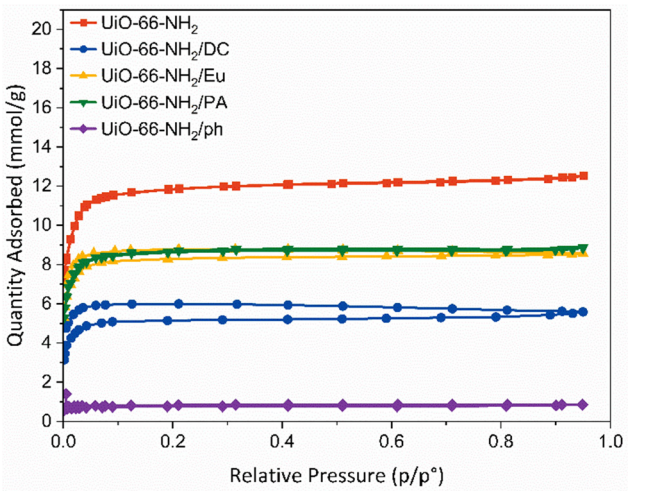

Fig. 2 N_2 gas sorption measurements performed at 77 K for pristine UiO-66-NH_2 (red) and its post-synthetically modified derivatives. UiO-66-NH_2/Eu (yellow), UiO-66-NH_2/PA (green), UiO-66-NH_2/DC (blue) and UiO-66-NH_2/ph (purple). Adsorption and desorption isotherms are denoted by filled and hollow symbols, respectively.

18.5 Å pore size, implying that it is filled with fragments of the enteric and organosilicon coatings. A broader Gaussian peak shape in the pore size at 16 Å indicates less gas entering the pores. The two micropores are preserved upon coating with a long-chain alkane, indicating that the coating of the alkane mostly occurs on the surface of the material. Unlike in the case of Eudragit RL® or DOWSIL™ coating, there are no bulky moieties in the PA, which may only result in a partial blockage of the larger pores. UiO-66-NH_2/ph demonstrates the greatest variation in pore size, with micropores of 13 Å, 16 Å, 18.5 Å and 21–24 Å determined. π–π stacking from the phenylsilane moieties may be creating additional pores within the framework material.

The interaction of the frameworks with CO_2 was examined using CO_2 adsorption experiments at 288, 298 and 308 K (Fig. 3 and Fig. S25, ESI†). At atmospheric pressure (1013.2 mbar), the adsorption of CO_2 was 1.99 mmol g^{-1}, which is comparable to that observed in the literature.[55,56] The isosteric heat of adsorption for pristine UiO-66-NH_2 was found to be 27.47 kJ mol^{-1}. Of greatest interest is the improvement of CO_2 uptake in the UiO-66-NH_2/Eu sample. The adsorption of CO_2 at 1000 mbar increased to 2.19 mmol g^{-1} and the isosteric heat of adsorption increased to 29.12 kJ mol^{-1}, which indicates moderate physisorption of CO_2. It is likely that the trimethylammonium moiety within the Eudragit RL® structure provides an additional site of interaction for CO_2. Although the highest heat of adsorption was recorded for the phenylsilane grafted derivative (31.57 kJ mol^{-1}), the significant reduction in CO_2 uptake to 0.61 mmol g^{-1} precludes its use as an enhanced CO_2 capture material.

Real time CO_2 separation from N_2 for each composite material was examined *via* fixed-bed column breakthrough experiments in a custom-made breakthrough rig, using a binary CO_2/N_2 mixture (50 : 50) (Fig. S26, ESI†). The GC was calibrated for the N_2 and CO_2 signal (Fig. S27, ESI†). N_2 breakthrough was first observed, prior to CO_2 (Fig. 3 and Fig. S28, ESI†). For pristine UiO-66-NH_2, the breakthrough point of N_2 was 6–8 min, with saturation reached at 10 min (Fig. S28a, ESI†). For CO_2 the breakthrough point was 8–10 min, while CO_2 saturation was reached at 26 min. UiO-66-NH_2/DC (Fig. S28b, ESI†), UiO-66-NH_2/Eu (Fig. 3), and UiO-66-NH_2/PA ((Fig. S28c, ESI†) all demonstrated improved separation between N_2 and CO_2 compared to the parent material. For UiO-66-NH_2/Eu, N_2 took longer to pass through the column than in the parent material, breaking through at 8–10 min and reaching saturation at 18 min. In comparison, the breakthrough point of CO_2 was 16–18 min, and saturation was reached at 22 min. The increased separation in the UiO-66-NH_2/Eu sample is consistent with the behaviour observed in the CO_2 isotherm. UiO-66-NH_2/Eu consistently demonstrated a higher uptake of CO_2 in the thermodynamic adsorption isotherm compared to the parent material, while functional quaternary amine groups in the enteric coating promoted improved interactions with CO_2. A practical CO_2 capacity of 0.98 mmol g^{-1} was calculated from the breakthrough curve. For UiO-66-NH_2/DC, the breakthrough point of N_2 was at 6–8 min, while saturation was reached at 14 min. The CO_2 breakthrough point was at 10–12 min while saturation was slowly reached at 32 min. A practical CO_2 capacity of 0.59 mmol g^{-1} was calculated from the breakthrough curve. The silyl functional groups improved the interaction of CO_2 with the material and did not greatly impact the CO_2 capacity of the composite at low partial pressures. UiO-66-NH_2/PA only demonstrated a small improvement in separation compared to the parent material. A practical CO_2 capacity of 0.54 mmol g^{-1} was calculated from the breakthrough curve. Each modified sample measurement displayed a roll-up feature,[57] indicating the concentration of the weaker sorbent $-N_2$ – briefly exceeds that of the feed. This is a common phenomenon in breakthrough curves for pure sorbent beds.[57]

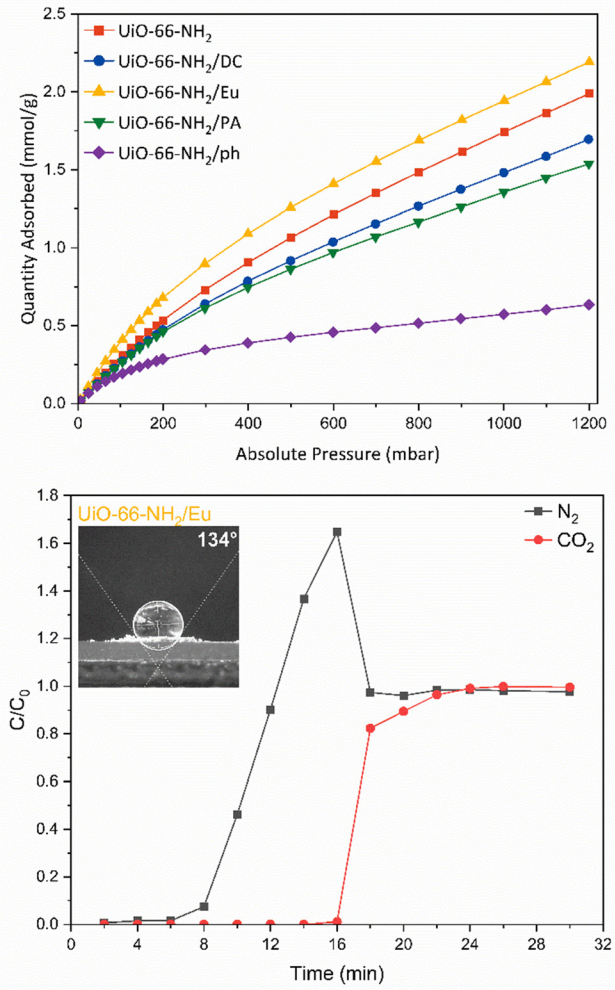

Fig. 3 CO_2 adsorption isotherms at 298 K of UiO-66-NH_2 (red), UiO-66-NH_2/DC (blue), UiO-66-NH_2/Eu (yellow), UiO-66-NH_2/PA (green) and UiO-66-NH_2/ph (purple) (above). Breakthrough calculations for UiO-66-NH_2/Eu for N_2 (black) and CO_2 (red). Inset: Water contact angle for UiO-66-NH_2/Eu (below).

Hydrophobicity studies. External hydrophobicity was tested through water contact angles onto the surface of a compacted sample. Pristine UiO-66-NH_2 yielded a contact angle of 0°, whereas the hydrophobically-modified samples demonstrated water contact angles of 134°, 129°, 138° and 112° for UiO-66-NH_2/Eu, UiO-66-NH_2/PA, UiO-66-NH_2/DC and UiO-66-NH_2/ph, respectively (a, Fig. S28, ESI†)). The modified materials were

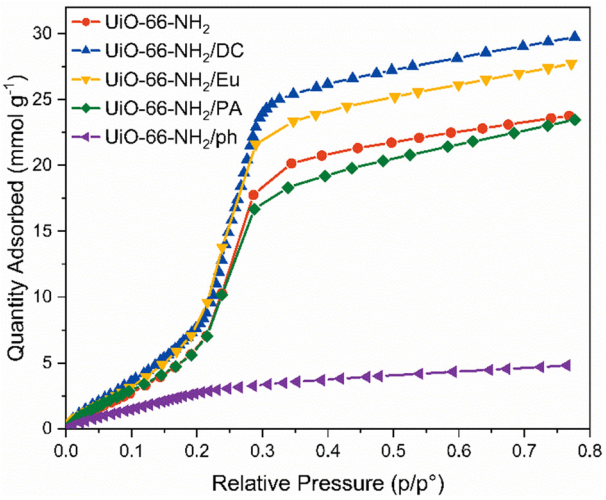

Fig. 4 Water vapour adsorption measurements performed at 298 K on pristine UiO-66-NH_2 (red), UiO-66-NH_2/DC (blue), UiO-66-NH_2/Eu (yellow), UiO-66-NH_2/PA (green) and UiO-66-NH_2/ph (purple).

shown to be externally hydrophobic, with the water droplet holding its shape for up to one hour after its placement on the compacted surface. N_2 gas sorption measurements were re-measured on wetted samples at 77 K to verify changes in surface area (Fig. S29, ESI†).

Internal hydrophobicity was initially tested through vapour sorption experiments (Fig. 4). Of all the materials, UiO-66-NH_2/ph demonstrated the lowest vapour uptake of 4.85 mmol g^{-1} at 76% relative humidity; however, this may be due to the reduced porosity calculated by the BET surface area and pore volume. Furthermore, there is a very gradual water uptake at low humidities, with typical S-shaped behaviour not observed.[58] The other candidate materials all showed similar H_2O vapour uptake performances as the pristine UiO-66-NH_2, which implied that the external hydrophobic coating does not improve the performance of the MOF under humid conditions. In some cases, the water vapour uptake increased from 20.4 mmol g^{-1} at 35% relative humidity in the pristine UiO-66-NH_2 to 23.5 mmol g^{-1} and 25.7 mmol g^{-1} in UiO-66-NH_2/Eu and UiO-66-NH_2/DC at 35% relative humidity, respectively. UiO-66-NH_2/PA demonstrated slight improvements in hydrophobicity at higher relative humidities. The water vapour uptake was reduced to 18.3 mmol g^{-1} at 35% relative humidity. There is little variation in hydrophobicity at low humidities. Interestingly, the increased uptake in vapour for Eu and DC may be due to the interactions displayed by the pristine polymers. Vapour sorption of these materials indicate H_2O uptake of up to 2.5 mmol g^{-1} at 80% relative humidity (Fig. S30, ESI†).

Conclusions

This project sought to investigate the impact of post-synthetically modifying UiO-66-NH_2 with hydrophobic functionalities to reduce the competition between CO_2 and H_2O in more industrially relevant conditions. Four broad, facile strategies (enteric coatings, long-chained alkane, organosilicon infiltration and phenylsilane grafting) were chosen, which led to four representative candidate materials of interest (UiO-66-NH_2/Eu, UiO-66-NH_2/PA, UiO-66-NH_2/DC and UiO-66-NH_2/ph). The post-synthetic modifications occurred under mild conditions and with short reaction times, which are conducive to a scalable process implementable in an industrial scenario. The post-synthetic modification was confirmed not to interfere with the structure of the parent material, as determined by PXRD, FT-IR, TGA and SEM characterisation.

Given that hydrophobicity in MOFs is generally characterised using water contact angles, alternative methods need to be developed to characterise hydrophobicity to vapour. Although these post-synthetically modified materials demonstrated external hydrophobicity, vapour sorption measurements revealed minimal impact on hydrophobicity when compared to the parent framework. Despite endowing the parent framework with an external hydrophobicity to liquid water, the modified frameworks were not sufficiently hydrophobic in the presence of humid air. The materials studied in this work demonstrate behaviour akin to that seen in Gore-Tex®; therefore, we propose the Gore-Tex® effect as a descriptor of this phenomenon.[59] Of the studied materials, the best coating performance was achieved using UiO-66-NH_2/Eu. Until now, MOF literature tends to use the water contact angle as a sufficient predictor of overall hydrophobicity.[60] This study indicates that such an assumption is not valid and that alternative methods are required to correctly characterise MOF hydrophobicity in an industrial setting. Nevertheless, we have demonstrated that we can improve the hydrophobicity of a MOF to liquid water, with efforts underway to expand the candidate MOFs that can be tested. There is also further interest in studying these materials which possess varied hydrophobicity for membranes where vapour transport is essential, *e.g.*, particular aquaporins.

Author contributions

DD developed the idea for this paper. DD, CK and MS supervised the experimental work. MS developed the initial optimisation strategies for each composite. KM, supported by MS, synthesised, and physically characterised bulk composite samples, including their gas and vapour sorption. Breakthrough experiments were performed by RL and JWH. KM and MS drafted the final paper, with input received from all authors.

Conflicts of interest

There are no conflicts to declare.

Acknowledgements

The authors acknowledge the funding provided by the Australian Research Council (JH and DD – DP230101901, CK – DP220103690, JH – FT210100589, RL – DE230100147). This project is also funded The University of Queensland Foundation

Research Excellence Awards. We gratefully acknowledge the technical and scientific assistance of Sydney Microscopy & Microanalysis, the University of Sydney node of Microscopy Australia. We wish to thank Mr Rohan Gillespie from Southern Green Gas Ltd. for discussions on hydrophobic porous materials. We would like to thank Prof. Chiara Neto for providing access to the goniometer for contact angle measurements, and Dr. Isaac Gresham for facilitating the measurements. We would like to thank Prof. Kim Chan for providing insights into enteric coatings. Finally, we gratefully acknowledge the support of Dr. David Dharma for setting up vapour sorption experiments.

Notes and references

1 H. Furukawa, K. E. Cordova, M. O'Keeffe and O. M. Yaghi, *Science*, 2013, **341**, 1230444.
2 K. Sumida, D. L. Rogow, J. A. Mason, T. M. McDonald, E. D. Bloch, Z. R. Herm, T. H. Bae and J. R. Long, *Chem. Rev.*, 2012, **112**, 724–781.
3 D. M. D'Alessandro, B. Smit and J. R. Long, *Angew. Chem., Int. Ed.*, 2010, **49**, 6058–6082.
4 T. C. Wang, W. Bury, D. A. Gomez-Gualdron, N. A. Vermeulen, J. E. Mondloch, P. Deria, K. Zhang, P. Z. Moghadam, A. A. Sarjeant, R. Q. Snurr, J. F. Stoddart, J. T. Hupp and O. K. Farha, *J. Am. Chem. Soc.*, 2015, **137**, 3585–3591.
5 O. K. Farha, I. Eryazici, N. C. Jeong, B. G. Hauser, C. E. Wilmer, A. A. Sarjeant, R. Q. Snurr, S. T. Nguyen, A. O. Yazaydin and J. T. Hupp, *J. Am. Chem. Soc.*, 2012, **134**, 15016–15021.
6 H. Konnerth, B. M. Matsagar, S. S. Chen, M. H. G. Prechtl, F. K. Shieh and K. C. W. Wu, *Coord. Chem. Rev.*, 2020, **416**, 213319.
7 S. Wu, H. Min, W. Shi and P. Cheng, *Adv. Mater.*, 2020, **32**, e1805871.
8 W. Zhang, Y. Hu, J. Ge, H. L. Jiang and S. H. Yu, *J. Am. Chem. Soc.*, 2014, **136**, 16978–16981.
9 S. M. Moosavi, A. Nandy, K. M. Jablonka, D. Ongari, J. P. Janet, P. G. Boyd, Y. Lee, B. Smit and H. J. Kulik, *Nat. Commun.*, 2020, **11**, 4068.
10 L. L. Huang, L. Yu, B. Li, B. B. Li, H. Wang and J. Li, *ACS Mater. Lett.*, 2022, **4**, 1053–1057.
11 M. Rubio-Martinez, C. Avci-Camur, A. W. Thornton, I. Imaz, D. Maspoch and M. R. Hill, *Chem. Soc. Rev.*, 2017, **46**, 3453–3480.
12 O. P. Murphy, M. Vashishtha, P. Palanisamy and K. V. Kumar, *ACS Omega*, 2023, **8**, 17407–17430.
13 N. Kumar, S. Mukherjee, N. C. Harvey-Reid, A. A. Bezrukov, K. Tan, V. Martins, M. Vandichel, T. Pham, L. M. van Wyk, K. Oyekan, A. Kumar, K. A. Forrest, K. M. Patil, L. J. Barbour, B. Space, Y. Huang, P. E. Kruger and M. J. Zaworotko, *Chemistry*, 2021, **7**, 3085–3098.
14 J. A. Mason, K. Sumida, Z. R. Herm, R. Krishna and J. R. Long, *Energy Environ. Sci.*, 2011, **4**, 3030–3040.
15 S. D. Kenarsari, D. L. Yang, G. D. Jiang, S. J. Zhang, J. J. Wang, A. G. Russell, Q. Wei and M. H. Fan, *RSC Adv.*, 2013, **3**, 22739–22773.
16 R. Krishna, *ACS Omega*, 2020, **5**, 16987–17004.
17 P. G. Boyd, A. Chidambaram, E. Garcia-Diez, C. P. Ireland, T. D. Daff, R. Bounds, A. Gladysiak, P. Schouwink, S. M. Moosavi, M. M. Maroto-Valer, J. A. Reimer, J. A. R. Navarro, T. K. Woo, S. Garcia, K. C. Stylianou and B. Smit, *Nature*, 2019, **576**, 253–256.
18 S. S. Kaye, A. Dailly, O. M. Yaghi and J. R. Long, *J. Am. Chem. Soc.*, 2007, **129**, 14176–14177.
19 S. Hausdorf, F. Baitalow, T. Böhle, D. Rafaja and F. O. R. L. Mertens, *J. Am. Chem. Soc.*, 2010, **132**, 10978–10981.
20 L. H. Xie, M. M. Xu, X. M. Liu, M. J. Zhao and J. R. Li, *Adv. Sci.*, 2020, **7**, 1901758.
21 B. Wang, X.-L. Lv, D. Feng, L.-H. Xie, J. Zhang, M. Li, Y. Xie, J.-R. Li and H.-C. Zhou, *J. Am. Chem. Soc.*, 2016, **138**, 6204–6216.
22 Y. S. Bae, J. Liu, C. E. Wilmer, H. Sun, A. N. Dickey, M. B. Kim, A. I. Benin, R. R. Willis, D. Barpaga, M. D. LeVan and R. Q. Snurr, *Chem. Commun.*, 2014, **50**, 3296–3298.
23 N. Ding, H. Li, X. Feng, Q. Wang, S. Wang, L. Ma, J. Zhou and B. Wang, *J. Am. Chem. Soc.*, 2016, **138**, 10100–10103.
24 X. Qian, F. Sun, J. Sun, H. Wu, F. Xiao, X. Wu and G. Zhu, *Nanoscale*, 2017, **9**, 2003–2008.
25 C. A. Fernandez, S. K. Nune, H. V. Annapureddy, L. X. Dang, B. P. McGrail, F. Zheng, E. Polikarpov, D. L. King, C. Freeman and K. P. Brooks, *Dalton Trans.*, 2015, **44**, 13490–13497.
26 A. X. Zhu, R. B. Lin, X. L. Qi, Y. Liu, Y. Y. Lin, J. P. Zhang and X. M. Chen, *Microporous Mesoporous Mater.*, 2012, **157**, 42–49.
27 D. D. Zu, L. Lu, X. Q. Liu, D. Y. Zhang and L. B. Sun, *J. Phys. Chem. C*, 2014, **118**, 19910–19917.
28 S. M. Cohen, *Chem. Rev.*, 2012, **112**, 970–1000.
29 D. Sun, P. R. Adiyala, S. J. Yim and D. P. Kim, *Angew. Chem., Int. Ed.*, 2019, **58**, 7405–7409.
30 A. von Wedelstedt, H. Chen, G. Kalies and R. Q. Snurr, *Langmuir*, 2020, **36**, 13070–13078.
31 M. De Toni, R. Jonchiere, P. Pullumbi, F. X. Coudert and A. H. Fuchs, *Chem. Phys. Chem.*, 2012, **13**, 3497–3503.
32 K. Jayaramulu, F. Geyer, A. Schneemann, Š. Kment, M. Otyepka, R. Zboril, D. Vollmer and R. A. Fischer, *Adv. Mater.*, 2019, **31**, 1900820.
33 P. Möder, H. Vierheilig, M. Alt and A. Wiemken, *Plant Soil*, 1993, **152**, 201–206.
34 J. H. Choe, J. R. Park, Y. S. Chae, D. W. Kim, D. S. Choi, H. Kim, M. Kang, H. Seo, Y.-K. Park and C. S. Hong, *Commun. Mater.*, 2021, **2**, 3.
35 J. G. Nguyen and S. M. Cohen, *J. Am. Chem. Soc.*, 2010, **132**, 4560–4561.
36 Y. Wan, D. Kong, F. Xiong, T. Qiu, S. Gao, Q. Zhang, Y. Miao, M. Qin, S. Wu, Y. Wang, R. Zhong and R. Zou, *Chin. J. Chem. Eng.*, 2023, **61**, 82–89.
37 Y. Wang, Z. Hu, T. Kundu, Y. Cheng, J. Dong, Y. Qian, L. Zhai and D. Zhao, *ACS Sustainable Chem. Eng.*, 2018, **6**, 11904–11912.

38 S. R. Wenger, E. R. Kearns, K. L. Miller and D. M. D'Alessandro, *ACS Appl. Energy Mater.*, 2022.
39 G. Kaur, J. Grewal, K. Jyoti, U. K. Jain, R. Chandra and J. Madan, in *Drug Targeting and Stimuli Sensitive Drug Delivery Systems*, ed. A. M. Grumezescu, William Andrew Publishing, 2018, pp. 567–626.
40 W. B. Liechty, D. R. Kryscio, B. V. Slaughter and N. A. Peppas, *Annu. Rev. Chem. Biomol. Eng.*, 2010, **1**, 149–173.
41 X. Lu, C. Huang, M. B. Lowinger, F. Yang, W. Xu, C. D. Brown, D. Hesk, A. Koynov, L. Schenck and Y. Su, *Mol. Pharm.*, 2019, **16**, 2579–2589.
42 D. G. Madden, A. B. Albadarin, D. O'Nolan, P. Cronin, J. J. T. Perry, S. Solomon, T. Curtin, M. Khraisheh, M. J. Zaworotko and G. M. Walker, *ACS Appl. Mater. Interfaces*, 2020, **12**, 33759–33764.
43 L. Feng, S. H. Lo, K. Tan, B. H. Li, S. Yuan, Y. F. Lin, C. H. Lin, S. L. Wang, K. L. Lu and H. C. Zhou, *Matter*, 2020, **2**, 988–999.
44 H. F. Zhang, M. Li, X. Z. Wang, D. Luo, Y. F. Zhao, X. P. Zhou and D. Li, *J. Mater. Chem. A*, 2018, **6**, 4260–4265.
45 P. Deria, J. E. Mondloch, E. Tylianakis, P. Ghosh, W. Bury, R. Q. Snurr, J. T. Hupp and O. K. Farha, *J. Am. Chem. Soc.*, 2013, **135**, 16801–16804.
46 H. X. Luo, F. W. Cheng, L. Huelsenbeck and N. Smith, *J. Environ. Chem. Eng.*, 2021, **9**, 105159.
47 Y. H. Cai, D. Y. Chen, N. J. Li, Q. F. Xu, H. Li, J. H. He and J. M. Lu, *ACS Sustainable Chem. Eng.*, 2019, **7**, 2709–2717.
48 J. Gu, J. Li and Q. Ma, *Nanomaterials*, 2022, **12**, 1134.
49 B. Yuan, G. Gou, T. Fan, M. Liu, Y. Ma, R. Matsuda and L. Li, *Angew. Chem., Int. Ed.*, 2022, **61**, e202204568.
50 C. Fang, C. L. Lu, M. H. Liu, Y. L. Zhu, Y. Fu and B. L. Lin, *ACS Catal.*, 2016, **6**, 7876–7881.
51 M. Thommes, K. Kaneko, A. V. Neimark, J. P. Olivier, F. Rodriguez-Reinoso, J. Rouquerol and K. S. W. Sing, *Pure Appl. Chem.*, 2015, **87**, 1051–1069.
52 S. Brunauer, P. H. Emmett and E. Teller, *J. Am. Chem. Soc.*, 1938, **60**, 309–319.
53 S. Y. Xu, Q. H. Gao, C. Zhou, J. X. Li, L. G. Shen and H. J. Lin, *Mater. Chem. Phys.*, 2021, **274**, 125182.
54 C. Gomes Silva, I. Luz, F. X. Llabres i Xamena, A. Corma and H. Garcia, *Chemistry*, 2010, **16**, 11133–11138.
55 X. Jiang, S. W. Li, S. S. He, Y. P. Bai and L. Shao, *J. Mater. Chem. A*, 2018, **6**, 15064–15073.
56 J. Winarta, B. H. Shan, S. M. Mcintyre, L. Ye, C. Wang, J. C. Liu and B. Mu, *Cryst. Growth Des.*, 2020, **20**, 1347–1362.
57 A. Kapoor and R. J. Yang, *AIChE J.*, 1987, **33**, 1215–1217.
58 M. R. Samarghandi, M. Hadi and G. McKay, *J Adsorption Sci.*, 2014, **32**, 791–806.
59 L. Hunter and J. Fan, *Textiles and fashion*, Elsevier, 2015, pp. 739–761.
60 Y. Li, H. T. Wang, Y. L. Zhao, J. Lv, X. Zhang, Q. Chen and J. R. Li, *Inorg. Chem. Commun.*, 2021, **130**, 108741.